Supplementary Material for
A *Pn* Magnitude Scale m_b(Pn) for Earthquakes along the Equatorial Mid-Atlantic Ridge

Won-Young Kim[1], Guilherme W. S. de Melo[2], and M. Assumpcao[3]

[1] Lamont-Doherty Earth Observatory, Columbia University, Palisades, NY 10964, USA
[2] GEOMAR Helmholtz Centre of Ocean Research Kiel, Kiel, Germany.
[3] Instituto de Astronomia, Geofísica e Ciências Atmosféricas, Universidade de São Paulo, São Paulo, SP, Brazil.

Contents

This supplemental material comprises a text, two tables, and eight figures.

Texts

Text S1. Variations of *Pn* propagation in St. Paul and Romanche transforms.

Tables

Table S1. List of Earthquakes Analyzed

Table S2. Inversion Results*

Figures

Figure S1. Attenuation curve for the Western part of the equatorial MAR, with 1,663 observed *Pn* peak amplitudes in nanometers.

Figure S2. Attenuation curve for the Eastern part of the equatorial MAR, with 378 observed *Pn* peak amplitudes in nanometers.

Figure S3. Comparisons of station corrections and V_S distribution at a 150 km depth, and station corrections versus lithosphere-asthenosphere boundary (LAB) depths.

Figure S4. Correlation of the event magnitude adjustments (EMA) with the lithospheric thickness in the St. Paul system and Romanche transform fault.

Figure S5. Comparison of the V_S distribution at 150 km depth and the amplitude-distance curves for western (towards Brazil) and eastern (toward African) paths.

Figure S6. Comparison of S-wave velocity distribution at 150 km depth from the tomography model SAM2019 (Celli *et al*. 2020) and *Pn* amplitude attenuation in the eastern and western sides of the equatorial MAR.

Figure S7. Comparisons of $m_b(Pn)$ and M_W values for 189 earthquakes with the event magnitude adjustment (EMA) and station corrections and without corrections.

Figure S8. Comparisons of $m_b(Pn)$ and M_W values for 189 earthquakes to examine the effect of station corrections.

References

Text S1. Variations of *Pn* propagation in St. Paul and Romanche transforms

St. Paul system and Romanche are two transform faults of the equatorial Atlantic, with different morphological and geodynamic features. St. Paul system is formed by four transform faults (Transform ***A, B, C, D***) offsetting ~630 km between the two Mid-Atlantic Ridge (MAR) axes (Maia et al. 2016), as seen in Fig. S4. The Romanche transform is another extensive and complex composed of two transform valleys: one that extends over the 900 km offset between the two MARs and the second located in a further north area, close to the east side ridge. St. Paul has different deformation styles along the four transform faults: Transform ***A*** contains a 200-km long and 30-km wide submarine stepover with a shear zone and local thrust faults uplifting rocks 1.5 mm/year above sea level in St. Peter and St Paul islets (Campos et al. 2010; Maia et al. 2016), while Transform ***C*** is composed of corrugated oceanic core complex features where detachment faults expose lower crust and mantle rocks (Vincent et al. 2023). Some authors suggested the presence of a different deformation between the two transform valleys of Romanche, with a possible more vertical motion in the north-side valley (Bonati 1978; Ligi et al. 2002). In parallel, Abercrombie & Ekström (2001) used teleseismic signals to analyze focal depths of earthquakes in Romanche and identified a difference between the earthquake depths comparing the east and west sides of the Romanche transform fault, the east side having deeper focuses. Other papers provide new contrasting features regarding the low-temperature mantle in the northern area of the Romanche (Bonatti et al. 1996; Maia et al. 2020), thick and serpentinized crust (Gregory et al. 2021), containing micro seismicity in that area with deformation reaching 34 km (Yu et al. 2021).

We plotted the magnitude adjustments of the strike-slip earthquakes along the St. Paul Romanche transform fault over the global lithospheric thickness modeled from Vs global tomography CAM2016 (Priestley et al. 2018, Fig.S3). In the St. Paul system, we observe a lithospheric thickness variation of ~8 km along the four transform faults. Most magnitude adjustments are positive in Transform ***A***, with some events presenting negative adjustments close to the west MAR axis or over the thrust faults, reflecting different contrasts in local lithospheric stress in that transform fault. Differently, most earthquake magnitude adjustments were negative in Transform **C**, with the existence of a reduced lithosphere thickness caused by the low-magma activity in oceanic core complexes close to the ridge axis (Vincent et al. 2023). As an effect, there is a difference in the Pn wave velocities (de Melo et al. 2021) and propagation in that area when compared to Transform *A*. In Romanche, the lithospheric thickness varies ~10 km between the two MAR axes. We observed that most negative magnitude corrections on the east side were located in the thinner zone of the CAM2016 model, with positive station corrections in the thicker lithospheric side. A possible explanation is the difference in the upwelling mantle melting between the east and west zones of the Romanche transform, collaborating with the existence of a variation in the Pn propagation along the Romanche transform with a complex lithospheric structure between the two MARs.

Tables.

Table S1. List of Earthquakes Analyzed*

Date	Time (hr:mn:s)	Lat (°N)	Long (°E)	h (km)	Mw	m_b(Pn)	N	F	EMA	Region†
2011 July 08	05:53:03	0.96	-26.42	10	5.64	5.30	11	S	-0.139	SPS
2011 July 27	23:00:30	10.80	-43.39	10	5.96	6.02	12	S	0.342	Vema
2011 July 28	16:11:58	4.14	-32.91	10	5.02	5.20	3	S	0.260	4-5ºN
2011 Aug 04	01:35:05	3.88	-32.15	10	5.18	5.43	9	S	0.591	Strakhov
2011 Aug 14	01:29:39	-1.34	-14.65	10	5.68	5.33	10	S	-0.342	Chain
2011 Nov 29	00:30:29	-1.60	-15.45	10	5.96	5.92	18	S	-0.023	Chain
2012 Feb 04	18:01:46	0.92	-26.75	10	5.28	5.50	17	S	0.428	SPS
2012 Feb 14	23:39:16	0.86	-29.23	10	5.33	5.31	17	S	0.177	SPS
2012 Mar 01	00:43:29	7.29	-36.00	10	5.36	5.15	11	S	-0.043	DSS
2012 Apr 07	20:37:51	1.05	-28.09	10	5.32	5.35	16	S	0.192	SPS
2012 Apr 10	05:09:08	-1.26	-13.97	10	5.90	5.73	19	S	-0.192	Chain
2012 May 06	05:54:05	12.70	-44.53	10	5.13	5.09	9	S	0.255	Marathon
2012 May 09	14:49:51	-0.96	-13.60	10	5.61	5.65	19	S	0.172	Chain
2012 July 12	04:04:12	-0.43	-19.77	10	5.22	5.16	9	S	0.076	Romanche
2012 Aug 16	12:08:17	7.32	-36.91	10	5.59	5.11	9	S	-0.320	DSS
2012 Aug 16	12:39:00	7.45	-36.55	10	5.39	5.21	7	S	-0.065	DSS
2012 Aug 16	14:14:30	-0.27	-18.76	10	5.35	5.50	5	S	0.485	Romanche
2012 Aug 17	00:12:10	-0.35	-18.71	10	5.24	5.39	7	S	0.392	Romanche
2012 Aug 31	00:35:35	3.81	-32.15	10	5.35	5.20	13	S	0.159	Strakhov
2012 Sept 24	00:55:52	0.75	-25.75	10	5.07	4.81	4	S	0.120	SPS
2012 Nov 03	12:58:12	7.05	-34.07	10	5.71	5.77	15	S	0.292	DSS
2012 Nov 04	20:02:56	7.75	-35.75	10	5.07	5.00	9	S	0.159	DSS
2013 Jan 15	23:58:58	-1.57	-15.63	10	5.05	5.21	9	S	0.089	Chain
2013 Jan 18	04:08:02	0.72	-25.40	10	5.00	4.93	19	S	0.100	SPS
2013 Jan 18	15:24:58	-1.39	-15.09	10	5.31	4.81	8	S	-0.494	Chain
2013 Feb 20	09:56:05	10.60	-41.04	10	5.11	4.92	6	S	0.032	Vema
2013 Mar 24	16:23:43	0.66	-25.88	10	5.10	4.91	9	S	-0.058	SPS
2013 Apr 01	20:01:12	1.25	-27.75	10	5.04	4.36	2	S	-0.404	SPS
2013 Apr 03	05:29:35	0.72	-27.14	10	5.24	5.13	15	S	-0.011	SPS
2013 May 31	10:19:27	0.83	-25.81	10	5.08	5.03	13	S	0.126	SPS
2013 June 24	22:04:13	10.70	-42.59	10	6.49	6.48	12	S	0.078	Vema
2013 Sept 05	04:01:36	15.21	-45.17	10	6.02	5.95	14	S	0.157	15-20
2013 Nov 14	14:06:23	3.87	-31.54	10	5.16	4.90	11	S	-0.017	Strakhov
2013 Dec 28	18:59:04	-1.37	-15.17	10	5.94	5.67	20	S	-0.276	Chain
2014 Jan 06	16:02:11	-1.12	-23.60	10	5.22	4.82	11	S	-0.258	Romanche
2014 Jan 24	02:35:28	-0.95	-13.02	9	5.28	4.93	5	S	-0.430	Chain
2014 Mar 11	17:42:01	0.59	-27.02	13	5.09	5.36	13	S	0.367	SPS

2014 Mar 18	07:11:40	0.75	-28.80	10	5.02	4.82	11	S	-0.018	SPS
2014 Mar 29	07:46:50	-0.85	-21.92	12	5.95	5.17	14	S	-0.626	Romanche
2014 Apr 30	15:52:40	-1.17	-13.46	10	5.81	5.36	9	S	-0.484	Chain
2014 May 24	11:49:26	0.69	-26.32	10	5.86	5.37	17	S	-0.426	SPS
2014 May 25	01:39:17	-1.02	-14.42	10	5.17	4.86	2	S	-0.017	Chain
2014 June 30	01:46:22	0.05	-17.34	10	5.68	5.64	19	S	0.022	Romanche
2014 July 01	12:39:06	8.70	-39.79	10	5.03	5.22	14	S	0.231	DSN
2014 July 01	20:49:14	0.78	-27.75	15	4.95	4.91	14	S	0.030	SPS
2014 Aug 10	12:12:24	0.75	-26.05	10	5.10	4.93	9	S	0.136	SPS
2014 Aug 13	10:07:28	0.84	-26.69	10	5.50	5.58	18	S	0.224	SPS
2014 Aug 22	13:02:35	6.85	-34.08	10	5.17	5.03	9	S	-0.041	DS
2014 Sept 16	03:44:13	0.86	-28.46	10	5.03	5.09	16	S	0.248	SPS
2014 Dec 27	22:31:18	-0.65	-20.74	10	5.01	5.04	9	S	0.198	Romanche
2014 Dec 28	17:24:40	0.75	-29.75	10	5.03	5.10	7	S	0.338	SPS
2015 Jan 26	07:32:26	0.75	-30.20	10	5.18	4.56	11	S	-0.409	SPS
2015 Feb 09	07:59:31	0.20	-17.13	10	5.15	5.35	18	S	0.350	Romanche
2015 Feb 24	06:54:48	1.00	-26.10	10	5.38	4.89	11	S	-0.403	SPS
2015 May 24	23:59:47	7.34	-36.39	10	5.36	5.52	19	S	0.265	DSS
2015 July 23	03:56:53	-0.69	-21.18	9	5.66	5.37	15	S	-0.255	Romanche
2015 Aug 06	21:36:58	0.81	-28.54	10	5.35	5.39	20	S	0.153	SPS
2015 Sept 18	15:59:42	15.28	-45.99	10	6.02	5.94	21	S	0.036	15-20
2015 Sept 28	07:41:44	3.77	-31.95	10	5.06	5.03	15	S	0.101	Strakhov
2015 Nov 14	05:25:35	7.22	-34.27	10	5.34	5.58	19	S	0.381	DSS
2015 Nov 24	20:45:02	-0.10	-17.83	10	5.61	5.67	21	S	0.077	Romanche
2015 Dec 28	19:24:15	-0.51	-19.96	10	5.13	5.03	12	S	0.095	Romanche
2016 Jan 27	15:11:17	1.02	-28.15	10	5.72	5.43	23	S	-0.218	SPS
2016 Feb 15	08:12:32	-1.40	-14.92	10	5.00	5.30	1	S	0.389	Chain
2016 Feb 21	01:04:26	8.06	-38.45	10	5.05	5.01	12	S	0.012	DSN
2016 Apr 01	14:25:54	-0.09	-17.55	12	5.01	5.31	7	S	0.420	Romanche
2016 Apr 27	17:14:14	-1.11	-13.83	10	5.16	4.56	1	S	-0.502	Chain
2016 May 07	16:07:08	-0.27	-18.94	10	5.12	5.39	11	S	0.468	Romanche
2016 May 28	04:43:30	7.39	-35.93	10	5.31	5.57	20	S	0.517	DSS
2016 July 24	14:10:51	0.92	-28.97	10	5.87	5.77	22	S	-0.059	SPS
2016 July 26	05:49:19	-0.27	-18.64	10	6.00	5.57	24	S	-0.382	Romanche
2016 Aug 18	10:49:19	-0.80	-21.32	10	5.32	5.03	4	S	-0.163	Romanche
2016 Aug 24	04:27:25	0.72	-29.93	10	5.05	5.15	12	S	0.172	SPS
2016 Aug 29	04:29:57	-0.05	-17.83	10	7.14	6.53	19	S	-0.534	Romanche
2016 Sept 14	09:18:25	-1.23	-14.31	10	5.02	4.80	1	S	-0.162	Chain
2016 Sept 28	22:12:13	0.02	-17.82	10	5.06	4.92	13	S	-0.052	Romanche
2016 Oct 05	20:53:39	7.14	-34.33	10	5.73	5.27	18	S	-0.347	DSS
2016 Oct 27	01:03:12	-1.51	-15.59	10	5.64	5.35	4	S	-0.293	Chain
2016 Nov 26	02:39:05	3.79	-32.10	10	5.23	5.34	12	S	0.446	Strakhov
2016 Dec 11	16:55:19	-0.37	-19.89	10	5.26	5.03	7	S	-0.158	Romanche

2017 May 01	11:08:18	0.37	-17.53	10	5.05	5.49	4	S	0.642	Romanche
2017 Aug 02	00:16:12	13.49	-49.34	10	5.28	5.39	16	S	0.508	NA-SA
2017 Aug 18	02:59:25	-1.11	-13.66	35	6.66	6.49	18	S	-0.298	Chain
2017 Oct 03	20:39:04	13.46	-49.33	10	5.66	6.20	18	S	0.750	NA-SA
2017 Oct 06	02:03:48	0.96	-25.51	10	5.60	5.11	9	S	-0.496	SPS
2017 Oct 16	18:08:29	1.12	-27.94	10	5.12	5.51	15	S	0.408	SPS
2017 Oct 19	22:23:27	7.40	-35.70	10	5.44	5.60	21	S	0.289	DSS
2017 Nov 30	06:32:50	-1.08	-23.43	10	6.50	6.46	22	S	0.072	Romanche
2018 Jan 26	13:29:13	1.76	-26.39	10	5.23	4.91	13	S	-0.267	SPS
2018 Feb 06	13:17:44	106	-43.27	10	5.35	5.17	6	S	-0.204	Vema
2018 Feb 15	08:27:22	-0.07	-17.84	10	5.60	5.60	18	S	0.107	Romanche
2018 Feb 20	00:53:04	-0.34	-19.87	10	5.41	5.16	13	S	-0.195	Romanche
2018 Mar 10	21:45:36	-1.42	-15.21	10	6.00	5.91	22	S	-0.164	Chain
2018 Mar 23	07:40:29	12.65	-44.57	10	5.61	5.50	18	S	0.081	Marathon
2018 May 23	05:44:43	7.44	-36.24	10	5.69	5.71	21	S	0.168	DSS
2018 May 24	23:11:47	0.82	-29.54	10	5.65	5.46	18	S	-0.153	SPS
2018 June 03	03:00:16	0.95	-26.56	10	5.17	4.92	17	S	-0.181	SPS
2018 June 14	18:12:15	0.85	-26.13	10	5.51	5.09	3	S	-0.467	SPS
2018 June 16	15:51:27	0.94	-28.33	10	5.08	5.31	15	S	0.268	SPS
2018 July 11	05:47:27	-1.49	-15.44	10	5.38	5.63	9	S	0.047	Chain
2018 July 23	10:35:59	-0.30	-19.25	10	5.98	5.54	17	S	-0.301	Romanche
2018 Aug 03	18:50:53	-0.87	-22.00	10	5.87	5.21	14	S	-0.524	Romanche
2018 Oct 07	00:10:04	7.66	-37.71	10	5.77	5.59	19	S	0.021	DSS
2018 Oct 16	08:35:36	0.95	-28.22	10	5.59	5.69	10	S	0.186	SPS
2018 Nov 10	07:17:52	0.83	-29.73	10	5.34	5.55	9	S	0.224	SPS
2018 Nov 27	12:03:27	-0.94	-13.83	10	5.74	5.63	10	S	-0.160	Chain
2018 Dec 31	20:45:30	15.29	-46.31	10	5.07	5.22	4	S	0.200	15-20
2019 Mar 23	12:35:24	7.53	-37.13	10	5.65	5.28	14	S	-0.208	DSS
2019 Mar 23	13:26:16	7.75	-37.25	10	5.11	4.95	3	S	-0.172	DSS
2019 Apr 13	15:23:15	0.67	-30.11	10	5.03	5.13	11	S	0.195	SPS
2019 Apr 30	20:52:22	15.30	-46.42	10	5.42	5.30	9	S	0.270	NA-SA
2019 June 17	20:03:11	0.82	-26.16	10	5.58	5.13	11	S	-0.220	SPS
2011 July 07	09:06:12	7.99	-38.06	10	5.03	4.91	5	N	0.034	DSS
2012 Jan 02	09:39:56	16.31	-46.54	10	5.03	5.09	3	N	0.374	NA-SA
2012 Jan 29	21:43:25	16.49	-46.53	10	5.31	4.92	6	N	-0.072	NA-SA
2012 Jan 29	21:54:20	16.62	-46.47	10	4.99	5.22	1	N	0.341	NA-SA
2012 Feb 14	04:03:58	0.60	-25.36	10	4.99	4.78	5	N	-0.198	RO-SPS
2012 Apr 04	12:10:48	7.41	-34.59	10	5.01	4.82	7	N	-0.082	DSS
2012 May 23	17:50:27	0.85	-27.61	10	5.26	5.09	10	N	-0.066	SPS
2012 May 28	09:36:08	9.57	-40.50	10	5.13	4.85	7	N	-0.142	Vema
2012 June 05	00:35:26	13.50	-44.85	10	5.28	5.19	9	N	0.065	15-20
2012 July 17	09:21:49	2.90	-31.20	10	4.98	4.87	2	N	-0.166	SPS-S
2012 July 28	16:01:11	4.55	-32.67	10	5.42	4.99	10	N	-0.468	4-5ºN

2012 July 28	16:18:46	4.51	-32.64	10	5.01	4.79	2	N	-0.170	4-5ºN
2012 Oct 04	23:14:56	17.44	-46.50	10	5.48	5.07	3	N	-0.061	NA-SA
2012 Oct 05	00:15:41	17.50	-46.45	10	5.40	5.06	2	N	-0.053	NA-SA
2013 Feb 18	00:29:56	5.59	-32.83	10	4.96	4.75	8	N	-0.254	4-5ºN
2013 Feb 18	03:40:48	5.54	-32.96	10	5.62	5.26	12	N	-0.387	4-5ºN
2013 Feb 18	04:40:07	5.74	-32.84	10	4.95	4.70	6	N	-0.341	4-5ºN
2013 Apr 14	09:51:08	15.44	-46.64	10	5.04	4.86	10	N	0.234	NA-SA
2013 July 22	22:15:10	-1.30	-15.99	10	5.21	5.22	2	N	0.158	Chain-RO
2013 July 22	22:19:05	-1.25	-15.98	10	5.34	5.02	3	N	-0.029	Chain-RO
2013 July 22	22:51:03	-1.25	-15.78	10	5.07	5.04	4	N	0.244	Chain-RO
2013 Sept 10	00:35:16	15.44	-46.72	9	5.25	5.10	8	N	0.247	NA-SA
2013 Oct 21	15:01:56	3.40	-31.40	10	4.97	5.13	1	N	-0.107	SPS-S
2013 Nov 04	14:39:34	9.00	-40.49	16	5.06	4.96	7	N	0.031	Vema
2014 Apr 14	07:47:32	4.04	-31.81	10	5.41	4.57	6	N	-0.635	Strakhov
2014 Apr 23	01:23:45	7.57	-36.73	10	4.96	5.02	9	N	0.117	DSS
2014 Apr 23	18:21:09	14.85	-45.02	10	5.33	5.26	12	N	0.036	15-20
2014 May 08	08:29:47	7.99	-38.03	10	4.96	4.93	7	N	0.020	DSS
2014 Sept 11	07:02:38	1.96	-30.64	10	5.17	5.21	8	N	-0.124	SPS-S
2014 Oct 19	19:51:10	8.70	-39.41	10	5.31	5.16	14	N	-0.198	DSN
2014 Oct 19	20:06:13	8.68	-39.33	10	5.39	5.11	12	N	-0.343	DSN
2014 Oct 19	23:58:56	8.73	-39.41	10	5.28	5.15	18	N	-0.225	DSN
2014 Oct 20	14:53:01	8.58	-39.39	10	5.01	5.19	14	N	0.115	DSN
2014 Nov 03	06:25:08	4.77	-32.65	10	4.96	5.19	9	N	0.023	4-5ºN
2014 Nov 03	07:18:08	4.63	-32.57	10	5.22	5.20	12	N	-0.192	4-5ºN
2014 Nov 03	08:23:53	4.67	-32.68	10	5.58	5.22	9	N	-0.445	4-5ºN
2014 Dec 02	01:37:15	5.61	-32.81	13	4.99	5.46	2	N	-0.021	4-5ºN
2015 Jan 04	21:23:15	14.51	-44.99	10	5.10	5.31	12	N	0.256	15-20
2015 Mar 12	15:23:25	8.06	-39.56	9	5.01	5.31	16	N	0.278	DSN
2015 Apr 18	09:08:41	8.06	-37.90	10	4.97	4.92	9	N	-0.003	DSS
2015 May 03	04:17:39	8.94	-40.46	10	5.09	5.28	15	N	0.237	Vema
2015 Oct 03	08:23:49	11.86	-43.74	10	5.10	4.96	4	N	-0.195	Vema
2015 Dec 12	23:30:34	0.69	-25.06	10	5.06	5.07	4	N	-0.061	RO-SPS
2015 Dec 18	11:46:48	-1.34	-15.83	10	5.53	5.56	14	N	0.221	Chain-RO
2016 Jan 07	10:50:31	-1.08	-15.95	10	5.08	5.00	2	N	0.210	Chain-RO
2016 Feb 20	12:33:42	4.45	-32.51	10	4.96	4.92	1	N	-0.018	4-5ºN
2016 Feb 20	12:48:06	4.57	-32.72	10	5.15	5.09	7	N	-0.128	4-5ºN
2016 Feb 20	13:22:08	4.75	-32.25	10	4.99	4.93	2	N	-0.200	4-5ºN
2016 Feb 20	13:50:49	4.63	-32.57	10	5.03	5.19	2	N	0.006	4-5ºN
2016 Feb 20	14:54:19	4.82	-32.59	10	4.96	5.36	4	N	0.174	4-5ºN
2016 Feb 20	14:59:58	4.49	-32.62	10	4.97	5.45	5	N	0.220	4-5ºN
2016 Feb 20	16:48:26	4.83	-32.63	10	5.02	5.16	3	N	0.040	4-5ºN
2016 Feb 21	02:26:21	4.51	-32.66	10	5.03	5.04	7	N	-0.133	4-5ºN
2016 Feb 27	02:41:46	4.53	-32.67	10	5.43	5.36	16	N	-0.152	4-5ºN

2016 Aug 05	17:40:32	14.58	-44.99	10	5.01	5.26	2	N	-0.020	15-20
2016 Aug 05	17:49:31	14.61	-45.10	10	5.42	5.34	12	N	-0.032	15-20
2016 Oct 20	00:09:26	13.31	-44.88	10	5.75	5.56	13	N	-0.158	15-20
2016 Oct 25	16:22:21	4.19	-32.53	10	5.05	4.96	3	N	-0.167	4-5ºN
2017 July 27	17:53:24	13.40	-49.33	10	6.01	6.19	17	N	0.456	NA-SA
2017 Nov 21	14:56:16	9.43	-40.53	10	4.95	5.13	12	N	0.238	Vema
2017 Dec 03	16:50:28	9.87	-40.64	10	5.02	5.15	6	N	0.114	Vema
2017 Dec 16	14:37:59	0.95	-27.73	10	5.30	5.03	14	N	-0.242	SPS
2017 Dec 28	11:20:43	5.55	-32.75	10	5.07	5.36	15	N	0.142	4-5ºN
2018 Jan 22	19:39:58	5.63	-32.88	10	5.04	5.15	9	N	0.012	4-5ºN
2018 Jan 26	07:28:34	16.16	-47.17	10	5.07	5.18	7	N	0.355	NA-SA
2018 Mar 25	11:11:53	8.08	-37.88	10	5.16	5.00	12	N	-0.147	DSS
2018 Apr 08	01:12:06	18.50	-47.65	10	5.02	4.95	2	N	0.183	NA-SA
2018 June 18	09:16:55	8.97	-40.40	10	4.95	5.17	1	N	0.033	Vema
2018 June 25	10:52:42	3.13	-31.30	10	5.46	5.25	11	N	-0.364	SPS-S
2018 Nov 17	13:17:59	15.54	-49.91	10	5.49	5.38	3	N	0.118	NA-SA
2018 Nov 18	16:04:23	14.93	-44.98	10	5.03	4.93	1	N	0.176	15-20
2018 Nov 27	19:34:45	15.57	-49.85	10	5.51	5.72	8	N	0.458	NA-SA
2019 Jan 23	14:48:29	7.98	-37.97	10	5.31	4.97	12	N	-0.112	DSS
2019 Feb 06	19:28:00	2.73	-31.12	10	5.06	4.79	9	N	-0.143	SPS-S
2019 Feb 25	15:05:33	4.29	-32.62	10	5.50	5.45	12	N	-0.032	4-5ºN
2019 Feb 25	15:47:35	4.31	-32.68	10	4.97	4.58	6	N	-0.226	4-5ºN
2019 Feb 25	16:04:08	4.25	-32.75	10	5.00	4.32	2	N	-0.824	4-5ºN

[*] h= focal depth in km, N=number of observations; F = focal mechanism (S=strike-slip, N=Normal faulting).

[†] Region: SPS = St. Paul system; RO-SPS = Romanche-St. Paul system; SPS-S= St. Paul system-Strakhov; DSS = Doldrums system – south; DSN = Doldrums system – north; 15-20 = Fifteen-Twenty, 4-5ºN = 4-5ºN; Chain-RO = Chain-Romanche; NA-SA = NA-SA plate boundary.

Table S2. Inversion Results*

	Nobs	**Nsta**	**Neve**	**b**	**K**	**Region**
West	1663	20	184	1.68	1.88	Equatorial MAR – Brazil
East	378	12	99	1.16	2.83	Equatorial MAR – Africa
All	2041	32		1.29	2.44	All Paths
N-Atlantic				1.86	1.62	100-1800 km

* Nobs = number of *Pn* amplitude measurements, Nsta = number of stations used, Neve = number of events analyzed, b = slope of amplitude-distance curve, K = constant relating mb(Pn) to Mw, plus attenuation beneath station, Region = applicable regions.

Figures.

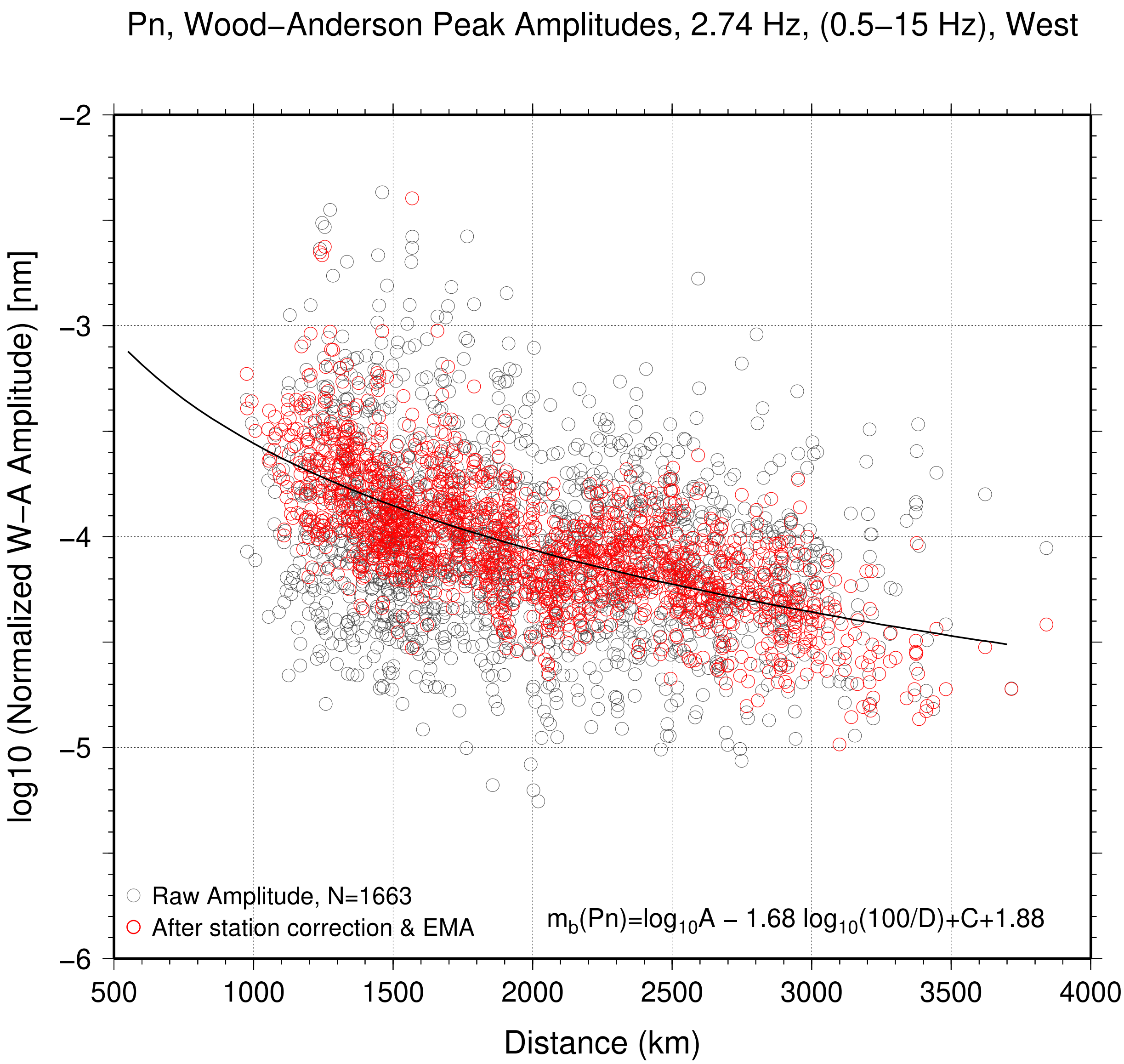

Figure S1. Attenuation curve for the Western part of the equatorial MAR, with 1,663 observed *Pn* peak amplitudes in nanometers. The logarithm of peak amplitude normalized by subtracting the event moment magnitude Mw is plotted with *gray circles*. The calculated peak amplitudes in the least-squares inversion – after making station corrections and event magnitude adjustments (EMAs) – are plotted by *red circles* for comparison. The thick solid line is the amplitude-distance curve of *Pn* waves in the Western part of the equatorial Atlantic region with parameters as in Table S1.

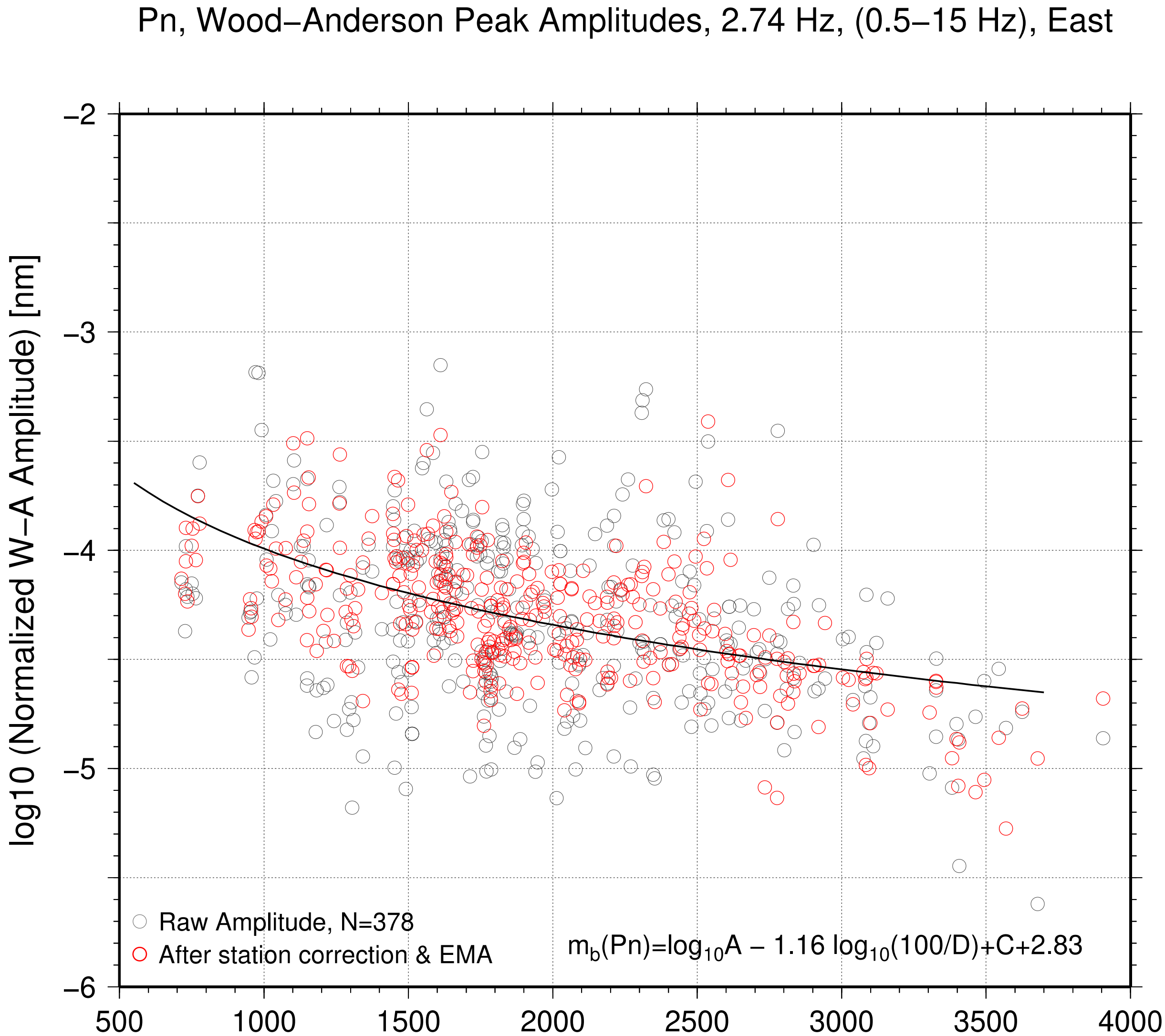

Figure S2. Attenuation curve for the Eastern part of the equatorial MAR, with 378 observed *Pn* peak amplitudes in nanometers. The logarithm of peak amplitude normalized by subtracting the event moment magnitude Mw is plotted with *gray circles*. The calculated peak amplitudes in the least-squares inversion – after making station corrections and event magnitude adjustments (EMAs) – are plotted by *red circles* for comparison. The thick solid line is the amplitude-distance curve of *Pn* waves in the Eastern part of the equatorial Atlantic region with parameters as in Table S1.

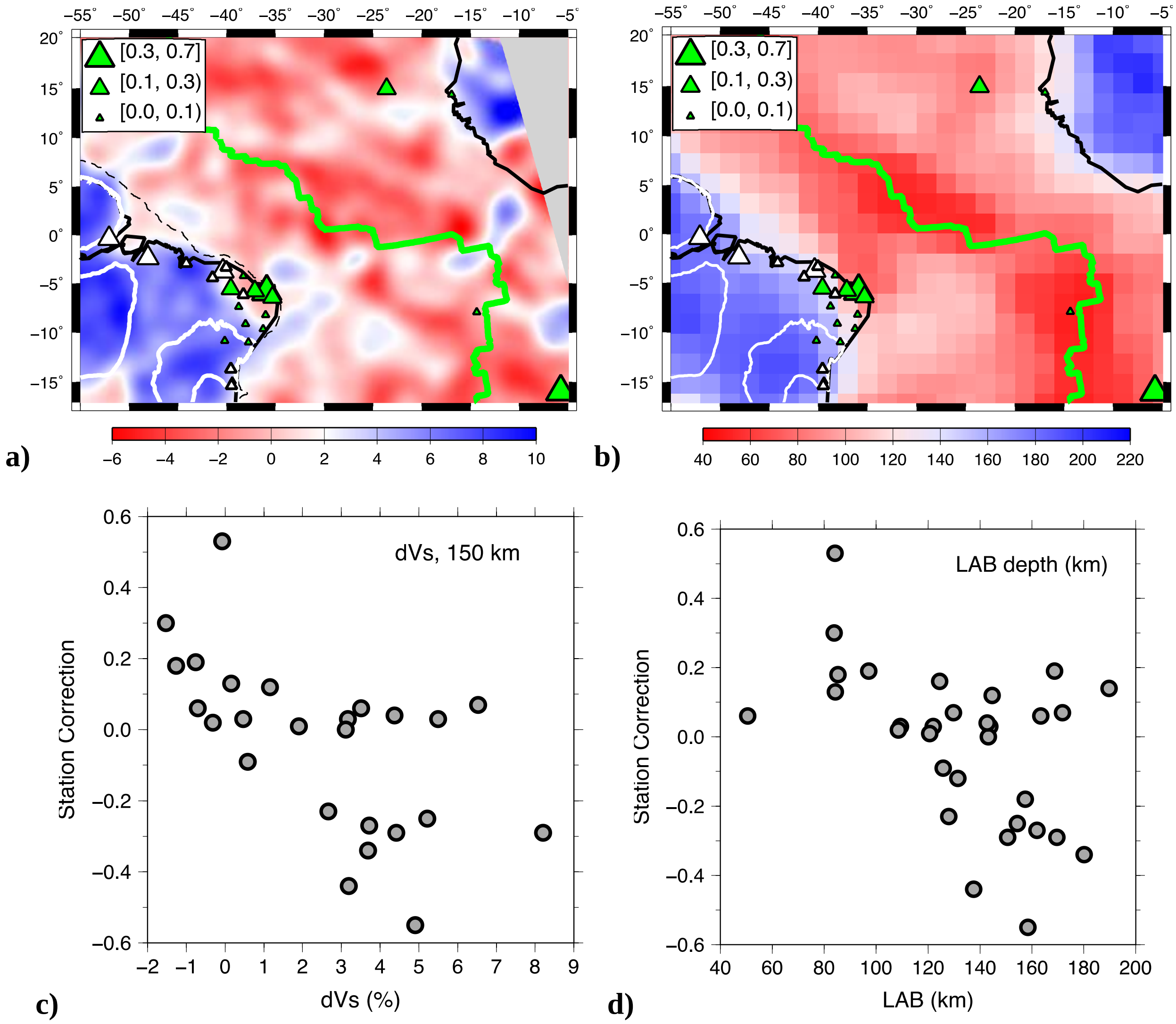

Figure S3. Comparisons of station corrections and V_S distribution at a 150 km depth, and station corrections vs lithosphere-asthenosphere boundary (LAB) depths. a) Map with station corrections and Vs anomalies at 150km depth from SAAM23 model (Ciardelli et al. 2022), b) same with LAB (Lithosphere/Asthenosphere boundary) depth from CAM2016 model (Priestley *et al*. 2018). In the maps, positive and negative corrections are indicated by green and white triangles, respectively. c) station corrections are plotted against Vs distribution. Linear regression yields a correlation coefficient of 0.60 with a standard deviation of 0.20 magnitude units, and d) station corrections are plotted against LAB depths. Linear regression yields a correlation coefficient of 0.53 with a standard deviation of 0.22 magnitude units.

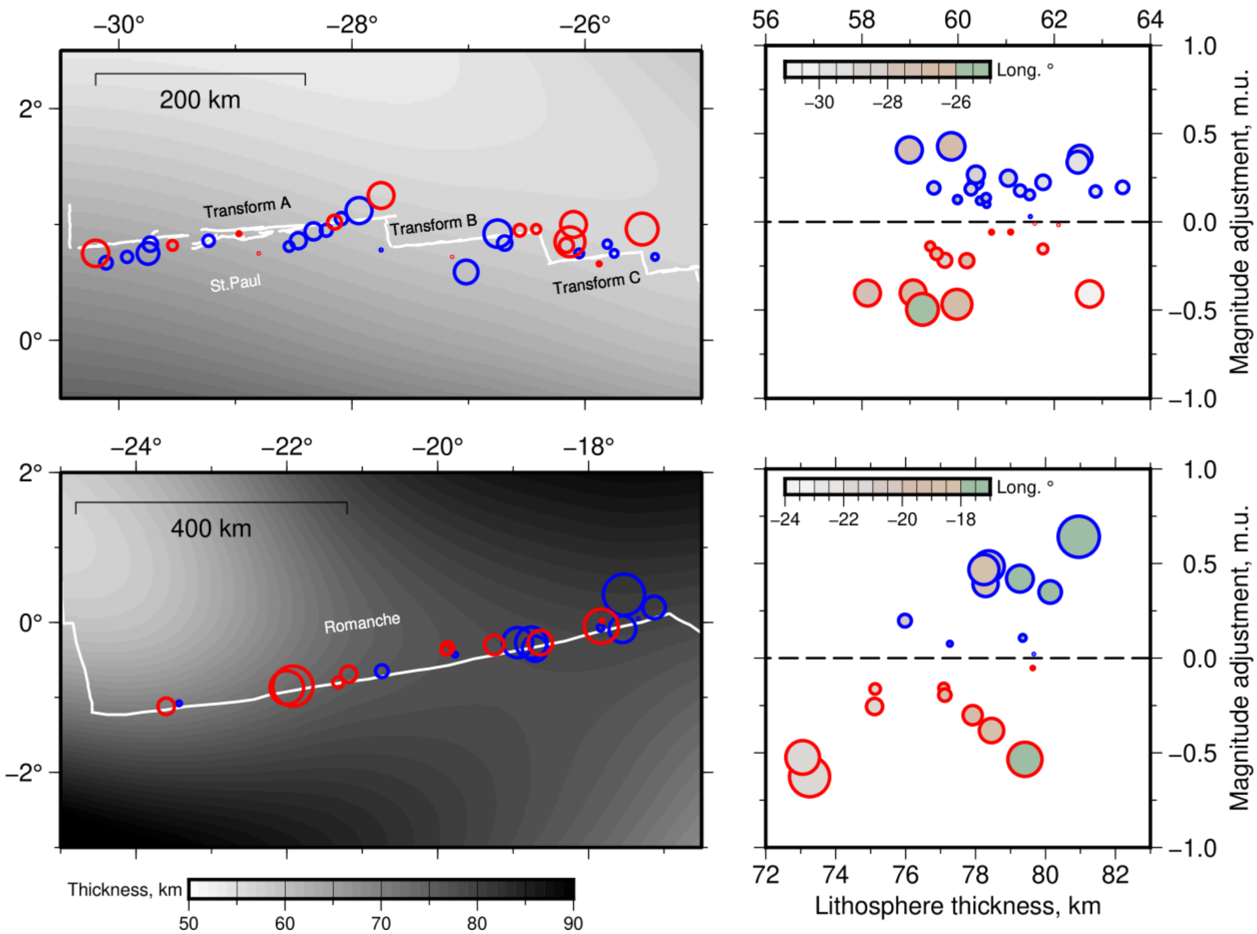

Figure S4. Correlation of the event magnitude adjustments with the lithospheric thickness in the St. Paul system and Romanche transform fault. (upper left panel) Event magnitude adjustments for all strike-slip earthquakes in the St. Paul system (bottom left panel) Event magnitude adjustments of earthquakes in Romanche transform fault. The red and blue circles represent the negative and positive magnitude adjustments, respectively. (upper right panel) correlation of the event magnitude adjustments (circles) with the lithospheric thickness of CAM2016 in the St. Paul system, (bottom right panel) correlation of the event magnitude adjustments (circles) with the lithospheric thickness of CAM2016 in the Romanche transform fault. Background shade is coded by the longitude coordinate of the epicenter location in the fault.

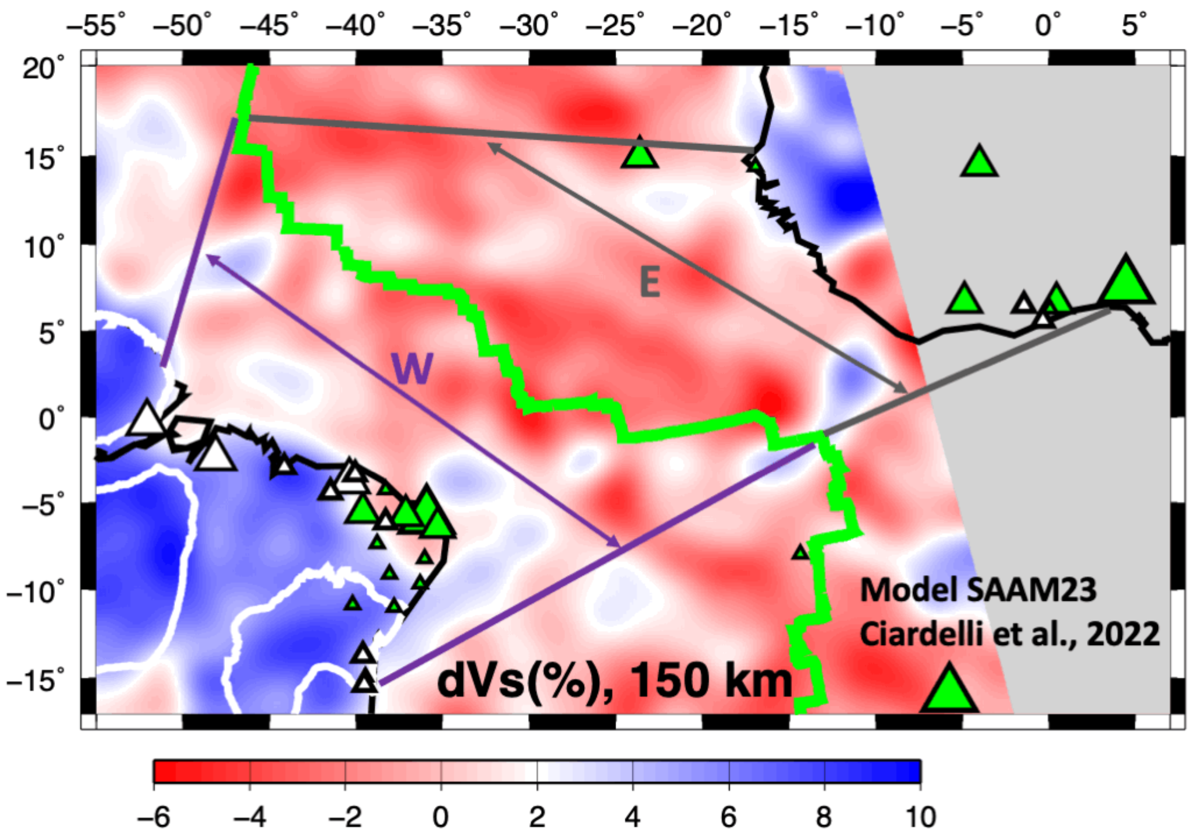

Fig. S5. Comparison of the V_S distribution at 150 km depth and the amplitude-distance curves for Western (towards Brazil) and Eastern (toward African) paths. S-wave anomaly map at 150 km depth from the tomography model SAAM23 (Ciardelli *et al*. 2022). The thicker violet and gray lines indicate the approximate limits of the paths from all earthquakes to the Brazilian and African coasts, respectively. Double arrows "W" and "E" show the average limits of each region. The Vs anomalies in the Western side (towards Brazil), on average, are not as low as compared with the Eastern side (towards Africa). This is consistent with the higher amplitudes observed in the amplitude-distance curves for the Western side of the equatorial Mid-Atlantic Ridge, compared with the curve for the Eastern paths (African side) shown in Figure 7 in the main text. The gray area in Africa is outside the minimum resolution of Model SAAM23 (Ciardelli *et al*. 2022).

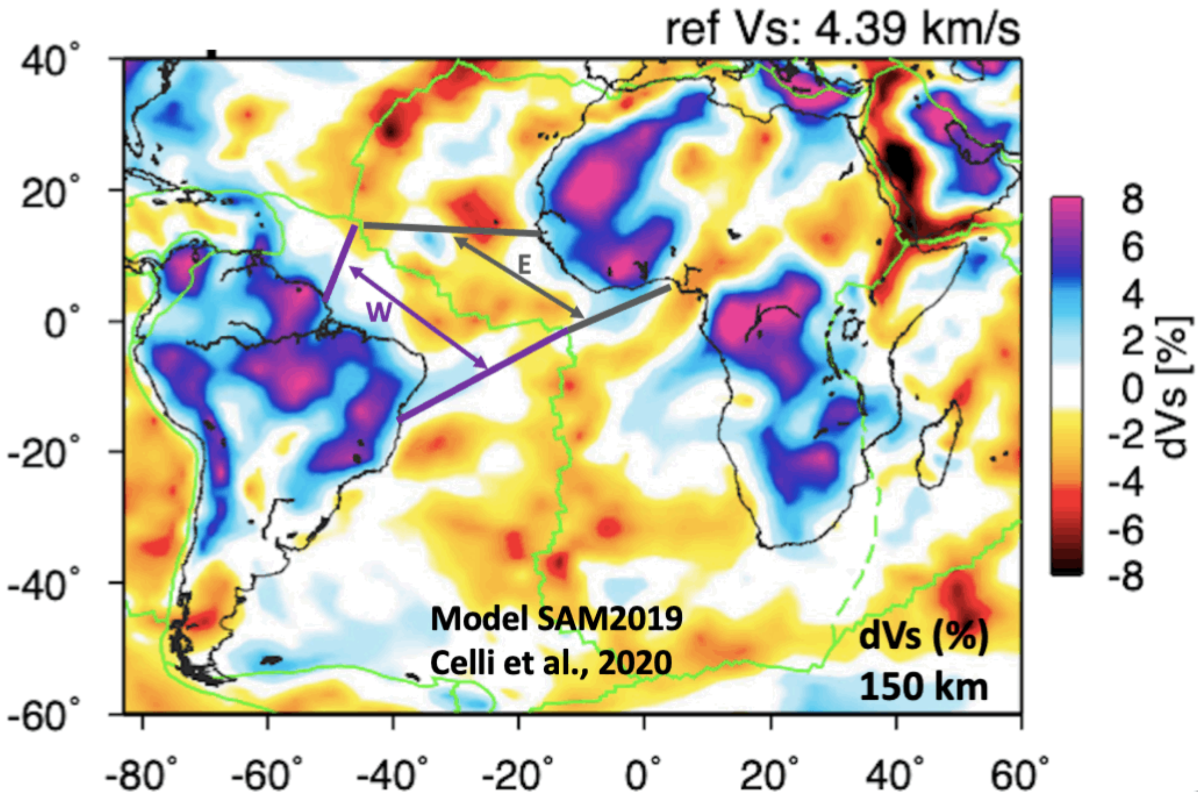

Figure S6. Comparison of S-wave velocity distribution at 150 km depth from the tomography model SAM2019 (Celli *et al*. 2020) and *Pn* amplitude attenuation in the eastern and western sides of the equatorial MAR. Lines as in Fig. S5. V_S is lower in the eastern side of the equatorial MAR, on average, compared to that of the western side. Lower *S*-wave velocities indicate stronger asthenosphere and probably higher attenuation. Figure based on Celli *et al.* (2020).

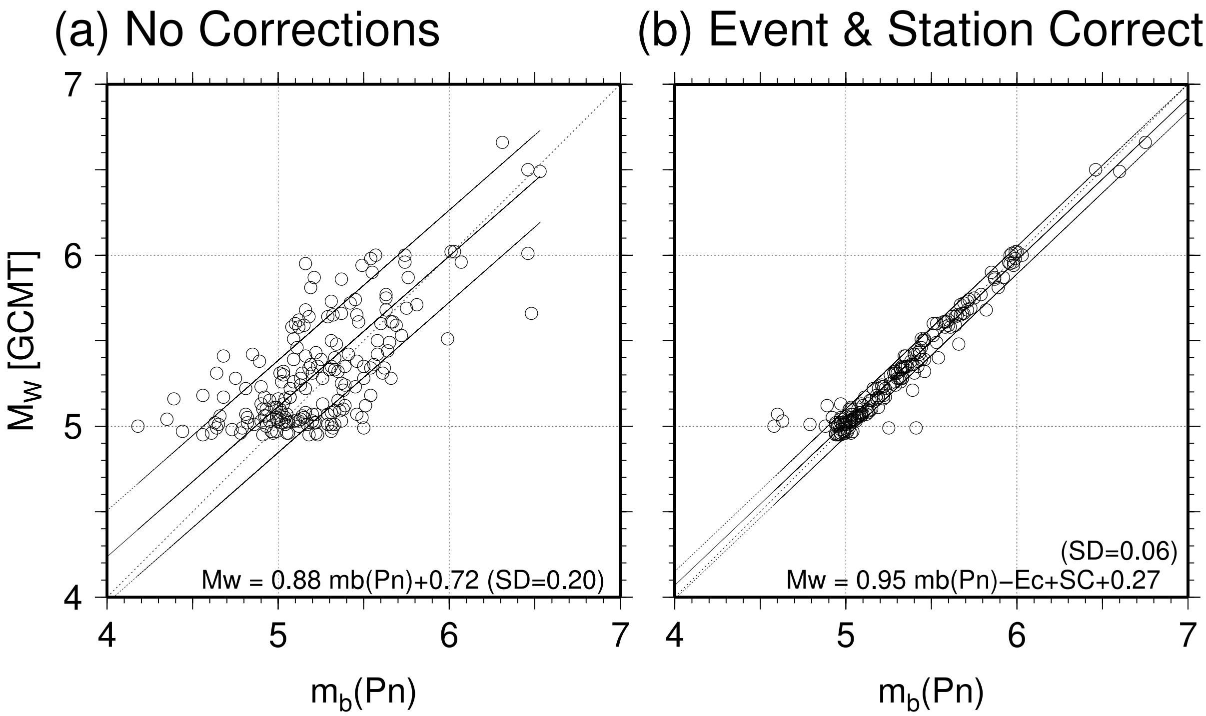

Figure S7. Comparisons of $m_b(Pn)$ and M_W values for 189 earthquakes. (a) $m_b(Pn)$ determined from the peak amplitude compensated only with the amplitude-distance curve. The regression line with a slope of 0.88 (*center solid line*) and lines of one orthogonal standard deviation of 0.20 magnitude units (*dashed lines*) are drawn. (b) $m_b(Pn)$ after making our event magnitude adjustment (EMA) and station corrections. The regression yields a slope of 0.95 with a standard deviation of only 0.06 magnitude units, indicating that an accurate approximation to the moment magnitude in the range from Mw 4.95 to 7.14 is given by our values of $m_b(Pn)$ once the magnitude adjustments (station and event corrections) are applied.

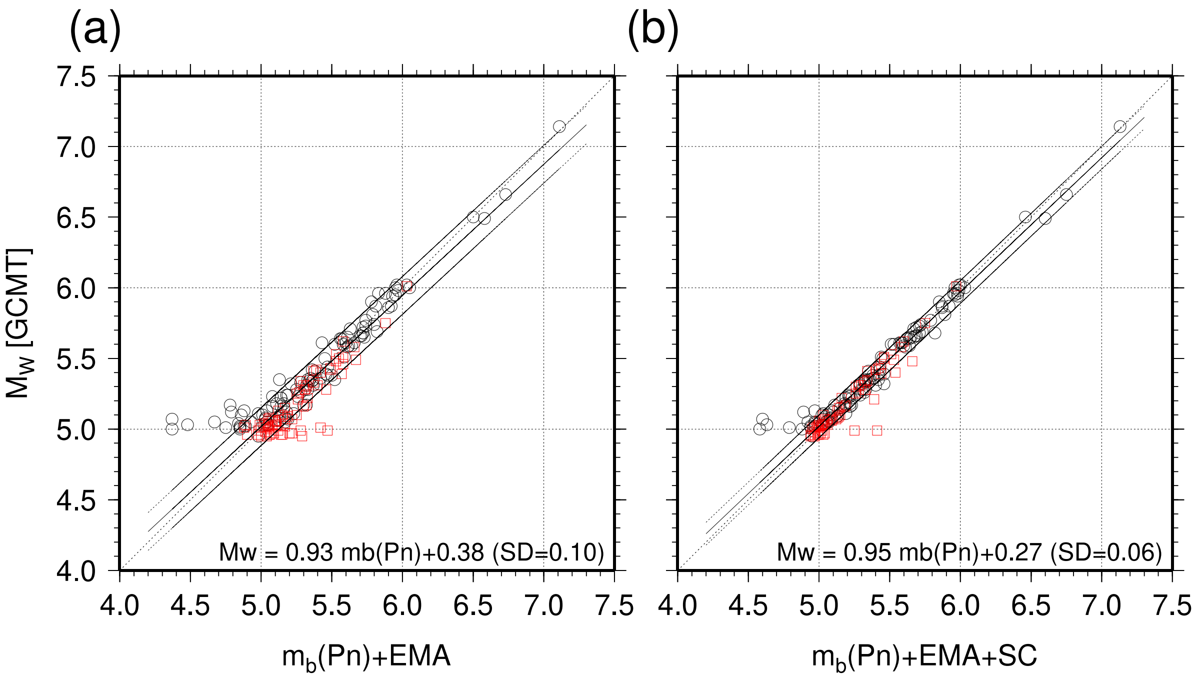

Figure S8. Comparisons of $m_b(Pn)$ and M_W values for 189 earthquakes to examine the effect of station corrections. (a) $m_b(Pn)$ determined by using event magnitude adjustment (EMA) but no station corrections. The regression yields a slope of 0.93 with a standard deviation of 0.10 magnitude units. Earthquake source types are indicated: normal (*circles*) and strike-slip (*red squares*). (b) $m_b(Pn)$ determined from the peak amplitude compensated with the amplitude-distance curve, event magnitude adjustment, and station corrections (SC). The regression line with a slope of 0.95 (*center solid line*) and lines of one orthogonal standard deviation of only 0.06 magnitude units (*dashed lines*) are drawn, indicating a reasonably weak effect of station corrections on the values of $m_b(Pn)$.

References.

Abercrombie, R. E., & Ekström, G., 2001. Earthquake slip on oceanic transform faults, *Nature*, **410,** 74-77.

Bonatti, E., 1978. Vertical tectonism in oceanic fracture zones, *Earth and Planetary Science Letters*, **37**, 369-379.

Bonatti, E., Ligi, M., Carrara, G., Gasperini, L., Turko, N., Perfiliev, S., & Sciuto, P. F., 1996. Diffuse impact of the Mid-Atlantic Ridge with the Romanche transform: An ultracold ridge-transform intersection, *J. Geophys. Res*., **101**, 8043-8054.

Campos, T. F., Bezerra, F. H., Srivastava, N. K., Vieira, M. M., & Vita-Finzi, C., 2010. Holocene tectonic uplift of the St Peter and St Paul Rocks (Equatorial Atlantic) consistent with emplacement by extrusion, *Marine Geology*, **271**, 177-186.

de Melo, G. W., Parnell-Turner, R., Dziak, R. P., Smith, D. K., Maia, M., do Nascimento, A. F., & Royer, J. Y., 2021. Uppermost mantle velocity beneath the Mid-Atlantic Ridge and transform faults in the Equatorial Atlantic Ocean, *Bull. Seismol. Soc. Am*, **111**, 1067-1079.

Gregory, E. P., Singh, S. C., Marjanović, M., & Wang, Z., 2021. Serpentinized peridotite versus thick mafic crust at the Romanche oceanic transform fault, *Geology*, **49**, 1132-1136.

Ligi, M., Bonatti, E., Gasperini, L., & Poliakov, A. N., 2002. Oceanic broad multifault transform plate boundaries, *Geology*, **30**, 11-14.

Maia, M., Sichel, S., Briais, A., Brunelli, D., Ligi, M., Ferreira, N., & Oliveira, P., 2016. Extreme mantle uplift and exhumation along a transpressive transform fault, *Nature Geoscience*, **9**, 619-623.

Maia, M., & Brunelli, D., 2020. The Eastern Romanche ridge-transform intersection (Equatorial Atlantic): slow spreading under extreme low mantle temperatures. Preliminary results of the SMARTIES cruise, In *EGU General Assembly Conference Abstracts* (p. 10314).

Vincent, C., Maia, M., Briais, A., Brunelli, D., Ligi, M., & Sichel, S., 2023. Evolution of a Cold Intra-Transform Ridge Segment Through Oceanic Core Complex Splitting and Mantle Exhumation, St. Paul Transform System, Equatorial Atlantic, *Geochemistry, Geophysics, Geosystems*, **24**, e2023GC010870.

Yu, Z., Singh, S. C., Gregory, E. P., Maia, M., Wang, Z., & Brunelli, D., 2021. Semibrittle seismic deformation in high-temperature mantle mylonite shear zone along the Romanche transform fault, *Science Advances*, **7**, eabf3388.